The Aeronautical Journal (2023), **127**, pp. 2023–2046
doi:10.1017/aer.2023.32

ROYAL AERONAUTICAL SOCIETY

REGULAR PAPER

Robust fault detection and diagnosis of primary air data sensors in the presence of atmospheric turbulence

S. Prabhu* and G. Anitha

Department of Aerospace Engineering, Division of Avionics, Madras Institute of Technology Campus, Anna University, Chennai, India
*Corresponding author. Email: vasanprabu155@gmail.com

Received: 2 August 2022; **Revised:** 25 January 2023; **Accepted:** 24 March 2023

Keywords: ADSS; IRU; INS/GPS; EW-AEKF; PADS-FDD; Residual; Turbulence

Abstract

This paper presents a fault detection and diagnosis (FDD) algorithm for various faults in the primary air data sensors (PADS) of an aircraft in the presence of external disturbances such as atmospheric turbulence. Rapid wind variations due to turbulence induce excessive error in the externally fitted air data probe measurements, which may lead to loss of control and misinterpretations by the flight crew. In adverse environmental conditions, the FDD of air data prefers robust and adaptive air data estimates that use an analytical redundancy approach with fewer computations. The proposed method considers the kinematics of the aircraft instead of the dynamics used in the state-of-the-art algorithms. The advantage of using kinematics is that it can reduce modeling errors significantly, avoiding high false alarm rates in the FDD process. For the estimation of stable and accurate air data under external disturbance, the inertial navigation system and global positioning system (INS/GPS) output are considered instead of actual air data probe or sensor measurements. The proposed algorithm uses estimates of air data using an exponentially weighted adaptive extended Kalman filter (EW-AEKF) to detect and diagnose PADS faults, which can perform well even in the presence of uncertain noise due to atmospheric turbulence experienced during flight. The simulation was carried out to validate the algorithm with flight data obtained from the X-Plane flight simulator under moderate atmospheric turbulence. The simulation experiments were carried out using the MATLAB programming platform. The results show that the proposed method achieves satisfactory FDD performance with lower root mean square error (RMSE) and computation time than traditional EKF-based algorithms.

Nomenclature

A	accelerometers output
a_x, a_y, a_z	acceleration components along body axes (m/sec^2)
AD	air data
AOA	angle-of-attack (rad)
AOSS	Angle-of-sideslip (rad)
A_x, A_y, A_z	specific force components
EW-AEKF	exponentially weighted adaptive extended Kalman filter
f, h	non-linear functions
FDD	fault detection and diagnosis
FDI	fault detection and isolation
g	gravitational acceleration (m/sec^2)
GPS	global positioning system
i	air data sensor index
IMU	inertial measurement unit
IRU	inertial reference unit
INS	inertial navigation system

J_T	threshold
k	time instant
p, q, r	body rotational rate components (rad/sec)
Q	process noise covariance matrix
R	measurement noise covariance matrix
PADS	primary air data sensors
RMSE	root mean square error
t	time (sec)
u_b, v_b, w_b	true airspeed velocity components (m/sec)
u	control input vector
U_g	ground speed (m/sec)
$U^b_{gx}, U^b_{gy}, U^b_{gz}$	ground speed velocity components along body axis (m/sec)
w & **v**	input and measurement noise vector
V_{wx}, V_{wy}, V_{wz}	wind velocity components in earth frame (m/sec)
U_t	true airspeed (m/sec)
V_w	wind speed (m/sec)
x & **z**	state and measurement vector
ω	rate gyros output
α	angle-of-attack sensor
β	angle-of-sideslip sensor
$\phi, \theta, \psi;$	attitude angles (rad)
$e_{Ut}, e_\alpha e_\beta$	residual signals of air data sensors
μ & σ	mean and standard deviation of error

1.0 Introduction

Reliability and health status monitoring of air data system sensor (ADSS) measurements are critical for the continuous operation and flight safety of aircraft that operate in the civil aviation sector. Faults on these sensors may vigorously lead to level A (catastrophic) failures. Since all the mechanical components of the sensor are exposed outside the aircraft's fuselage, they can be affected by environmental anomalies such as clogging, icing at high altitudes and airflow disruptions due to external disturbances such as atmospheric turbulence. At high altitudes, the high-density ice crystals may not be able to be tackled by the conventional heater mechanisms of air data probes such as Pitot probes and wind vanes (α and β vanes), etc. The atmospheric turbulence during flight can produce low-to-heavy fluctuations in the air data measurements, which may lead to poor decision-making by the pilot. Moreover, malfunctions in the primary air data sensors, such as airspeed, angle-of-attack (α), and angle-of-sideslip (β) will affect the aircraft's performance and control. Some of the tragic accidents that happened in the past due to air data sensor failures are evidence of the impact of faulty air data sensors on civil aircraft flight control laws. The Pitot tubes of Air France's flight number AF447 were affected by accumulated ice crystals at a high altitude, which led to the aerodynamic stall. In the recent past, the two consecutive accidents of the well-known Boeing 737 Max-8 flight suspected a synchro-based electromechanical sensor (AOA) fault that wrongly indicated and activated the Maneuvering Characteristics Augmentation System (MCAS) used to provide the pitch augmentation control law to the aircraft [1–3]. Therefore, the estimation and availability of air data parameters are critical to ensure the safety of a flight and its passengers. The conventional approach depends on the availability of redundant air data sensors, where the air data parameters are measured and faulty sensor measurements are voted out using a voter circuit. However, all the air data probes are subjected to the same environmental conditions, which may lead to common-mode failure followed by the wrong output to the sensor fault-tolerant control system (FTCS). Based on the history of the accidents, it is evident that the redundant air data sensors are vulnerable to adverse environmental conditions. In the case of the AF447 crash, all the redundant airspeed sensors faulted, followed by a common-mode failure and a failure of de-icing mechanisms in the presence of extreme weather conditions such as high-altitude icing. The main reason for the crash of the Boeing

https://doi.org/10.1017/aer.2023.32 Published online by Cambridge University Press

737 Max 8 was a lack of redundancy in the pitch augmentation system, which depended only on a single AOA sensor measurement. For the monitoring of malfunctions in the redundant air data sensors, a robust model-based approach with analytical sorts of measurements and reduced modeling errors is highly preferred to increase the availability of air data in all flight conditions and to perform an effective FDD in the presence of external disturbances. In general, an FDD of aircraft sensors is the problem of autonomously detecting the presence, isolating the location, and identifying the type and severity of the faults [4]. The block diagram presented in Fig. 1 shows the kinematic model-based estimation of air data parameters and air data sensor FDD, where the input commands provided by the inertial reference unit (IRU) measured linear accelerations (A_x, A_y, A_z) and angular rates (p, q, r) instead of flight control surface inputs [5]. As can be noticed, only the blocks within the blue dashed line are run onboard, and they are free from the influence of the sensor faults. The faults are injected into the recorded air data measurements and diagnosed by the FDD block offline. There have been several studies carried out on the fault detection and diagnosis (FDD) of air data sensors. The air data and inertial system FDI were performed using a consolidation module and Kalman filter, which depend on the availability of redundant sensors to compute the algorithm [6]. There are some approaches that provide analytical redundancy when a simultaneous fault on a cluster of ADSS occurs [7,8]. The enhanced FDI algorithm with model- and signal-based approaches was proposed with multiple AOA sensor fault cases that used the IMU measurements [9]. However, the dependence on flight control system inputs may not guarantee robustness against system uncertainties. Some researchers proposed observer-based sensor fault detection schemes with an analytical redundancy approach [10]. Due to the observer-based schemes, it may not be able to provide a reliable output when the sensor noise increases during abrupt wind variations. A physical-analytical redundancy approach was proposed by Antonio et al. [11] to estimate the aircraft flow angles (AOA and AOSS). Since it considers several evaluation processes, the computational burden may increase. Recently, the estimation of aircraft parameters along the longitudinal axis was studied considering faults in the sensors of the air data system using Kalman filters [12,13]. Zahed et al. [14] developed virtual sensors to detect faults in the airspeed and AOA sensors using the extended Kalman filter (EKF) in the X-Plane flight simulator environment. However, the use of flight controls as inputs will induce additional errors in the aircraft dynamics that cannot be tackled by the traditional EKF-based algorithms. More recently, an air data FDI using machine learning was proposed using real flight data [15]. With increasing demand for technological innovations, the high-fidelity digital twin approach was proposed [16]. However, these methods cannot provide robustness against external disturbances. Other researchers have proposed air data estimation in the presence of a wind field with the help of the Kalman filter [17]. The Kalman filter (EKF) used for the estimation framework cannot deal with increased system noise when the aircraft experiences atmospheric turbulence. Recently, Mohamed and Joy [18] proposed the estimation of AOA and AOSS using an adaptive EKF under atmospheric turbulence. Other researchers proposed the air data FDD in the presence of atmospheric turbulence using the unscented Kalman filter (UKF) with real flight data from civil jet aircraft [19]. However, the computational load due to UKF is not affordable for the mathematically intensive civil transport aircraft. From the above methods, it is obvious that the challenging part of an air data sensor FDD that uses a model-based approach is reducing the model uncertainty and improving the robustness against external disturbances with less computation. In this paper, a robust FDD algorithm for primary air data sensors (PADS) on commercial aircraft with less computation is proposed. This is possible because the aircraft kinematics use modified equations of motion that do not consider stability and control derivatives. In other words, the kinematics of an aircraft, which do not consider the forces and moments of the aircraft, are considered. In addition, the adaptive version of the extended Kalman filter is used to estimate stable and accurate air data in the presence of external disturbances such as atmospheric turbulence. The mathematical model is developed with the knowledge of aircraft kinematic relations and air data system parameters, considering inputs from the specific forces (A_x, A_y, A_z) and angular rates (p, q, r) measured by the inertial reference unit (IRU) to reduce the system complexity. All the sensor measurements used in the algorithm, such as the IRU and ground speed velocity components, are readily available from the X-Plane sensor data output option. The estimation framework considers inputs to the mathematical

https://doi.org/10.1017/aer.2023.32 Published online by Cambridge University Press

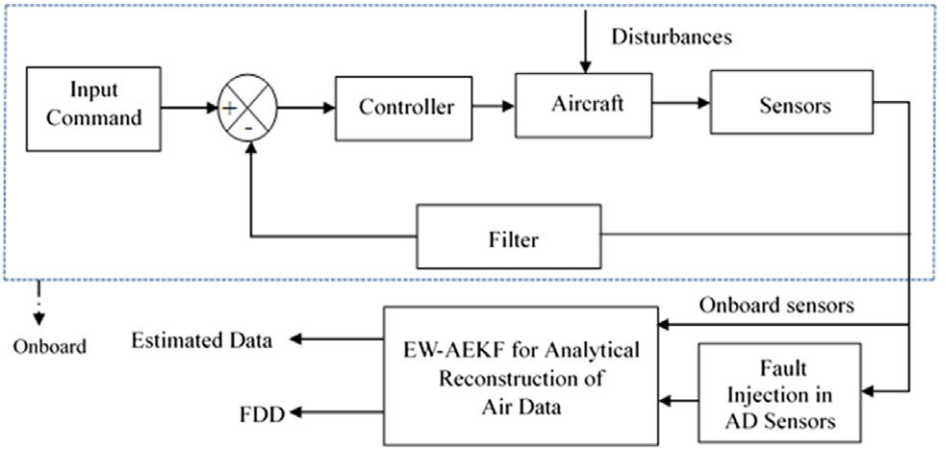

Figure 1. *Air data sensor FDD using kinematics.*

model from IRU and outputs from ground velocity components (INS/GPS) to estimate true airspeed (U_t) and airflow angles, namely angle-of-attack (α) and angle-of-sideslip (β). The specific reason behind the selection of ground velocity components for the air data estimation is their lower sensitivity to external influences such as atmospheric turbulence and other disturbances. The proposed mathematical model tackles the modeling errors and the external disturbances with the estimation framework provided by the exponentially weighted adaptive extended Kalman filter (EW-AEKF). The filtering process using EW-AEKF does not consume large amounts of computation since the mathematical model was developed with a lower state vector dimension and the adaptive process was done under the sliding time moving window (N), which reduces the estimation error and computational load in the presence of atmospheric disturbance (turbulence).

This paper is structured as follows: The problem statement that highlights the determination of residual signals in model-based FDD and air data in civil aircraft is outlined in Section 2. Section 3 defines the kinematic model required for the estimation of air data parameters and the estimation framework developed for the proposed algorithm. The relationship between the kinematic model and air data components is presented first. Then, the state-space representation of the model and the air data estimation using an adaptive version of EKF are established. The fault detection logic, the modelling of the sensor faults, and the rationale behind the design of FDD thresholds are presented in Section 4. Section 5 presents the experimental setup and simulation results of estimation performance, robustness analysis using Monte Carlo simulations, and various fault scenarios of air data sensors using flight data obtained from the X-Plane flight simulator under atmospheric turbulence conditions. Concluding remarks are presented in Section 6.

2.0 Problem statement

In general, model-based FDD techniques of ADSS are evaluated through the residual signals, which represent the inconsistency between the actual system behavior and the mathematical model of the system. For the sensor FDD of the proposed method, it can be defined as the difference between true air data sensor measurements and the estimated air data. The key advantages of using residuals are their ease of implementation and the fact that they carry exact information about faults such as stuck, bias, drift, increased noise faults, etc. It can be determined as,

$$e(k) = z_k - \hat{z}_k \tag{1}$$

where $e\ (k)$ is the residual value at the k^{th} time step, z_k is the true sensor measurements, and $\hat{z}_k$ is the estimated measurement of the filter, such as an extended Kalman filter [20]. The kinematic model-based

https://doi.org/10.1017/aer.2023.32 Published online by Cambridge University Press

primary air data sensors FDD (PADS-FDD) proposed in this paper consider the residuals of each sensor category of the air data system. Since the above Equation (1) is the generic form of residual signals, a complete knowledge of the signals and underlying dynamics is required to provide good cross-platform portability [21]. The residuals used in this FDD algorithm are presented as follows,

$$\begin{cases} e_{U_t} = U_t - \hat{U}_t \\ e_\alpha = \alpha - \hat{\alpha} \\ e_\beta = \beta - \hat{\beta} \end{cases} \tag{2}$$

where U_t, α, β are air data system components (true airspeed, AOA, and AOSS) and e_{U_t}, e_α, $e_\beta$are the residuals of true airspeed, AOA, and AOSS, respectively. The calculated residuals are used to monitor each sensor's health status robustly. The air data is adaptively estimated, and residuals are generated by the adaptive version of the EKF, namely the EW-AEKF. The predetermined thresholds are fixed to detect various faults on the sensors. A fault occurs when residuals exceed the thresholds and are detected using the detection logic (discussed in Section 5).

In this study, we tested various fault scenarios for air data sensors that include freezing (stuck) fault, bias, drift and increased noise faults. To detect every fault efficiently, the threshold values are carefully determined, considering the sensor's impact on the aircraft's performance and control. In practice, the allowable error limit for sensors on civil aircraft is defined by civil aviation authorities such as the Civil Aviation Authority (CAA, UK), the European Aviation Safety Agency (EASA), the Federal Aviation Administration (FAA), etc. For example, the airspeed error limit that is allowable as per EASA's Certification Specifications (CS 25.1323) of subpart F is $\pm$ 3% or $\pm$ 2.5m/s [22,23]. With this knowledge, the details of fixed thresholds are presented in Section 5 of this paper. In order to implement robust and reliable fault detection (PADS-FDD), we used the available sensor measurements other than the redundant air data (AD) sensor measurements. More clearly, the proposed AD estimation and FDD algorithm use measurements from the IRU and an integrated INS/GPS navigation system, which is less sensitive to external disturbances and readily available on the air data and inertial reference system (ADIRS) of modern aircraft. The following relationships are used to compute the air data from the estimated parameters. Using the velocity triangle relationship, one can extract the true airspeed as presented by,

$$U_g = U_t + V_w \tag{3}$$

where U_g is the ground speed measured in the earth frame, U_t is the true airspeed measured in the aircraft body frame, and V_w is the wind speed measured in the earth frame. The true airspeed can be written in component form by using airspeed and airflow angles as,

$$\begin{cases} u = U_t \cos\alpha \cos\beta \\ v = U_t \sin\beta \\ w = U_t \sin\alpha \cos\beta \end{cases} \tag{4}$$

To extract the true airspeed without the aid of redundant Pitot tube measurements of the air data system, the Equation (3) is rewritten with a direction cosine matrix [24] as,

$$U_t = \mathbf{C}_e^b U_g - V_w^b \tag{5}$$

where $\mathbf{C}_n^b$ is the transformation matrix from the earth frame to the body frame, and V_w^b is the wind speed represented in the body frame. The airflow angles of the aircraft air data system are computed using the following relationship using body-axis velocity components:

$$\begin{cases} \alpha = \tan^{-1}\left(\dfrac{w_b}{u_b}\right) \\ \beta = \sin^{-1}\left(\dfrac{v_b}{U_t}\right) \end{cases} \tag{6}$$

https://doi.org/10.1017/aer.2023.32 Published online by Cambridge University Press

where α is the angle-of-attack, β is the angle-of-side slip, and u_b, v_b, and w_b are the airspeed velocity components represented in the aircraft body frame. In Section 3, we will present the mathematical model for air data estimation.

3.0 Kinematic model and AD estimation

Kinematic models are indeed a special form of the general equations of motion (EOM) of an aircraft, for which specific forces (the outputs of accelerometers in the center of gravity) and angular rates serve as inputs. They can conveniently be written in state-space form. An aircraft EOM takes the form of three sets of first-order differential equations, one each for translational velocities, angular velocities, and attitude angles [25]. For the air data estimation of the proposed work, we considered only the differential equations of velocities and attitude angles. The main advantage of a kinematic model is that it does not take inputs from flight control surface deflections (rudder, elevator and aileron) and is free from modeling uncertainties that degrade the model-based sensor FDD algorithms. Using the customary body-fixed reference frame, the equations for the components u, v, and w of true airspeed (U_t) along the body axes take the following form:

$$\begin{cases} X = m(\dot{u} + qw - rv) + mg\sin\theta \\ Y = m(\dot{v} + ru - pw) - mg\cos\theta\sin\phi \\ Z = m(\dot{w} + pv - qu) - mg\cos\theta\cos\phi \end{cases} \tag{7}$$

where p, q, and r denote the rotational rates about the aircraft body frame; θ and ϕ denote the pitch and roll angles, respectively; m denotes the aircraft mass; and g denotes the local acceleration due to gravity. X, Y and Z represent the components of the total aerodynamic forces, including the aerodynamic effects of propulsion systems. The aircraft kinematic-based model is driven by specific forces measured by ideal accelerometers and rotational rates measured by rate gyroscopes. In flight, such ideal accelerometers would measure the specific aerodynamic forces according to:

$$\begin{cases} X = A_x m \\ Y = A_y m \\ Z = A_z m \end{cases} \tag{8}$$

where A_x, A_y, and A_z denote the specific aerodynamic forces along the aircraft body axes. On substituting Equation (8) into Equation (7) by eliminating the mass 'm' of the aircraft, we get

$$\begin{cases} \dot{u} = a_x + vr - wq - g\sin\theta \\ \dot{v} = a_y - ur + wp + g\cos\theta\sin\phi \\ \dot{w} = a_z + uq - vp + g\cos\theta\cos\phi \end{cases} \tag{9}$$

The above set of equations represents the kinematical relations of aircraft velocities. The other set of equations is that governed by the first-order differential equations for the attitude (Euler) angles in the earth-fixed reference frame and is presented by

$$\begin{cases} \dot{\phi} = p + q\sin\phi\tan\theta + r\cos\phi\tan\theta \\ \dot{\theta} = q\cos\phi - r\sin\phi \\ \dot{\psi} = q\sin\phi\sec\theta + r\cos\phi\sec\theta \end{cases} \tag{10}$$

The above Equations (9) and (10) can be called the kinematic model required for the estimation of air data. The development of a robust air data model is further enhanced with available sensor measurements, such as IRU and INS/GPS, to guarantee the reliability of estimation. Using Equation (9), the velocity dynamics required for the proposed method is written in kinematical form as

https://doi.org/10.1017/aer.2023.32 Published online by Cambridge University Press

$$\begin{cases} \dot{U}^b_{gx} = a_x + U^b_{gy} r - U^b_{gz} q - g \sin\theta \\ \dot{U}^b_{gy} = a_y - U^b_{gx} r + U^b_{gz} p + g \cos\theta \sin\phi \\ \dot{U}^b_{gz} = a_z + U^b_{gx} q - U^b_{gy} p + g \cos\theta \cos\phi \end{cases} \tag{11}$$

whereU^b_{gx}, U^b_{gy}, U^b_{gz} are the ground speed velocity components transformed from the earth frame to aircraft's body frame which are readily available from the flight simulator sensor data set (in the earth frame). The above velocity dynamics include the effects of wind variations represented in the aircraft body frame. With the knowledge of Equations (10) and (11), the rest of the paper will focus on estimation of air data using the above kinematic relations. Note that the ground speed components U_{gx}, U_{gy}, U_{gz} are readily available from the flight sensor data of aircraft, either from flight simulation or real flight. Hence the output equations are presented as,

$$\begin{aligned} U_t &= \sqrt{{U_{tx}}^2 + {U_{ty}}^2 + {U_{tz}}^2} \\ \alpha &= \tan^{-1}\left(\frac{U_{tz}}{U_{tx}}\right) \\ \beta &= \sin^{-1}\left(\frac{U_{ty}}{U_t}\right) \end{aligned} \tag{12}$$

where U_{tx}, U_{ty}, and U_{tz} are the true airspeed components computed using the ground velocities and wind velocities in the body frame. Using Equations (4) and (11), the dynamics of air data variables $[U_t, \alpha, \beta]^T$ i.e., $\dot{U}_t$, $\dot{\alpha}$, and $\dot{\beta}$ can be obtained as,

$$\dot{U}_t = \dot{U}^b_{gx} \cos\alpha \cos\beta + \dot{U}^b_{gy} \sin\beta + \dot{U}^b_{gz} \sin\alpha \cos\beta \tag{13}$$

$$\dot{\alpha} = \frac{\dot{U}^b_{gz} \cos\alpha - \dot{U}^b_{gx} \sin\alpha}{U_t \cos\beta} \tag{14}$$

$$\dot{\beta} = \frac{-\dot{U}^b_{gx} \cos\alpha \sin\beta + \dot{U}^b_{gy} \cos\beta - \dot{U}^b_{gz} \sin\alpha \sin\beta}{U_t} \tag{15}$$

From the above information, the non-linear state-space model for the proposed AD estimation with the kinematics of the aircraft can be presented as,

$$\begin{aligned} \dot{\mathbf{x}}(t) &= f[\mathbf{x}(t) + G(\mathbf{x}(t))\ (\mathbf{u}(t) + \mathbf{w}(t))] \\ \mathbf{z}(t) &= h(\mathbf{x}(t)) \\ \mathbf{z}_m(t) &= [h(\mathbf{x}(t)) + \mathbf{v}(t)] \end{aligned} \tag{16}$$

where $\mathbf{x}$ represents the state vector, $\mathbf{u}$ represents the input vector, $\mathbf{z}$ represents the measurement vector, and $\mathbf{w}$ and $\mathbf{v}$ represent the process and measurement noise vectors with zero-mean Gaussian with covariance matrices $\mathbf{Q}$ and $\mathbf{R}$, respectively. f and h are the non-linear functions. The variables of system equations are written as follows:

$$\mathbf{x} = [U_t, \alpha, \beta, \phi, \theta, \psi]^T \tag{17}$$

$$\mathbf{u} = [A, \omega]^T + \mathbf{w} \tag{18}$$

$$\mathbf{z} = \left[U_t, \alpha, \beta, \phi, \theta, \psi\right]^T + \mathbf{v} \tag{19}$$

where $A = [a_x, a_y, a_z]^T$ is the output of accelerometers, and $\omega = [p, q, r]^T$ is the rate gyroscope output of the IRU or IMU. The air data variables, including true airspeed, angle-of-attack (α), angle-of-side slip (β) and attitude angles (ϕ, θ, ψ;) are represented by the state vector ($\mathbf{x}$). The input vector ($\mathbf{u}$) represents the IRU output along the body axes. The measurement vector ($\mathbf{z}$) represents the measured velocities along the x, y, and z axes transformed into body axes and attitude angles provided by the INS/GPS

https://doi.org/10.1017/aer.2023.32 Published online by Cambridge University Press

navigation system. The process noise vector ($\mathbf{w}$) consists of three elements, such as the input noise components of accelerometers ($\mathbf{w}^A$), input noise components from rate gyros ($\mathbf{w}^\omega$) and the random process noise of wind velocities ($\mathbf{w}^{Vw}$), which is given by

$$\mathbf{w} = \begin{bmatrix} \mathbf{w}^A & \mathbf{w}^\omega & \mathbf{w}^{Vw} \end{bmatrix}^T \tag{20}$$

Due to the random nature of the unknown disturbance (turbulence), it is difficult to predict the local wind field variations. Moreover, considering wind velocity as a state will increase the computational burden. The wind velocity due to turbulence is considered as a random walk process model. Note that, the wind velocity due to turbulence is considered as an unknown input to the system, and it can be isolated when there is no requirement of existence conditions. It is assumed to be a Gaussian random process whose covariance can be estimated. When the noise level of the process varies intensely, an optimal wind estimation is required to calculate accurate air data. Hence, the random variation of wind velocities due to turbulence was captured using EW-AEKF and is represented as

$$\dot{V}_w = [\dot{V}_{wx}\ \dot{V}_{wy}\ \dot{V}_{wz}]^T = \mathbf{w}^{Vw} \tag{21}$$

where V_{wx}, V_{wy}, and V_{wz} are the components of wind velocities represented in the earth frame, and they can be transformed into the body frame using the transformation matrix. The proposed work assumed that all the sensors were fault-free throughout the PADS-FDD process, except the redundant air data sensors. Specifically, the operation of the inertial measurement unit (IMU) that includes the rate gyro sensors (p, q, r) and accelerometers (a_x, a_y, a_z) is assumed fault-free throughout the PADS-FDD, and the noise variations of all the sensors are reduced by the EW-AEKF. In wind disturbance conditions, the EW-AEKF adaptively tuned the noise covariance of the IMU. Hence, the noise effects of rate gyros and accelerometers are well-tackled for the reliable estimation of air data, including U_t, α and β.

3.1 Estimation framework of EW-AEKF

The optimality of traditional extended Kalman filter (EKF) algorithms depends on the a priori noise statistics of process noises and measurement noises ($\mathbf{Q}$ and $\mathbf{R}$) of sensors. Prabhu and Anitha [26] presented the air data FD using an iterated optimal extended Kalman filter (IOEKF) with the standard deviations provided by the manufacturer of the sensors. However, in the case of large variations in the sensor measurements caused by external disturbances, the known process noise ($\mathbf{Q}$) cannot provide satisfactory performance for the air data estimation using IOEKF. Usually, the choice of $\mathbf{Q}_{k\text{-}1}$ made by the trial-and-error method may induce additional uncertainty due to the user's expertise and background [27]. As such, the selection of the process noise covariance matrix is a challenging part of using the traditional EKF algorithms. To resolve this issue, an adaptive version of EKF is proposed that can automatically tune the noise statistics of sensors. In this case, a computationally effective nonlinear filter such as the exponentially weighted adaptive extended Kalman filter (EW-AEKF) is considered for the estimation of air data to present the PADS-FDD algorithm. The more general form of an EKF filtering algorithm is presented as follows:

Step 1: Initialisation

$$\begin{cases} \hat{\mathrm{x}}_0 = E(\mathrm{x}_0) \\ \mathrm{P}_0 = E((\mathrm{x}_0 - \hat{\mathrm{x}}_0)(\mathrm{x}_0 - \hat{\mathrm{x}}_0)^T) \end{cases} \tag{22}$$

Step 2: Prediction

$$\begin{aligned} \hat{\mathrm{x}}_{k/k-1} &= \mathrm{F}_{k,k-1}\hat{\mathrm{x}}_{k-1} + \mathrm{G}_{k-1}\mathrm{u}_{k-1} \\ \mathrm{P} &= \mathrm{F}_{k,k-1}\mathrm{P}_{k-1}\mathrm{F}_{k,k-1}^T + \mathrm{Q}_{k-1} \end{aligned} \tag{23}$$

Step 3: Correction

$$\begin{aligned} \mathrm{K}_k &= \mathrm{P}_{k/k-1}\mathrm{H}_k^T[\mathrm{S}_k]^{-1} \\ \hat{\mathrm{x}}_k &= \hat{\mathrm{x}}_{k/k-1} + \mathrm{K}_k[\mathrm{v}_k] \\ \mathrm{P}_k &= (\mathrm{I} - \mathrm{K}_k\mathrm{H}_k)\mathrm{P}_{k/k-1} \end{aligned} \tag{24}$$

https://doi.org/10.1017/aer.2023.32 Published online by Cambridge University Press

In Equation (22), $\hat{\mathbf{X}}_0$ and $\mathbf{P}_0$ are the estimated initial state and state error covariance matrices, respectively. In Equation (23), $\mathbf{F}_k$ is the state transition matrix, $\mathbf{G}_k$ is the control input matrix; $\mathbf{u}_k$ is the control input vector; and $\mathbf{Q}_k$ represents the process noise covariance matrix. In Equation (24), $\mathbf{K}_k$ is the Kalman gain matrix, $\mathbf{H}_k$ is the measuring matrix. $\mathbf{S}_k$ is the innovation covariance, and $\mathbf{v}_k$ represents the measurement noise with the covariance matrix, $\mathbf{R_k}$. The residual e_k is defined as the difference between true measurements and its estimated values available at time step k, and it can be presented as

$$e_k = \mathrm{z}_k - \mathrm{H}_k \hat{\mathrm{x}}_{k/k-1} \tag{25}$$

The theoretical covariance of innovation sequence ($\mathbf{C}_{ek}$) is presented by

$$\mathrm{C}_{ek} = E\left[e_k e_k^T\right] \tag{26}$$

Using the maximum likelihood estimation (MLE) approach, the noise covariance can be estimated and adjusted adaptively from the measurements with the maximum probability approach. As stated in the MLE procedure, if $k < N$, the ideal value of the estimated $\mathbf{C}_{ek}$ in a moving time window is presented by

$$\hat{\mathrm{C}}_{ek} = \frac{1}{N}\sum_{j=j_0}^{k} e_j e_j^T \tag{27}$$

where N is the size of the moving time window, $j_0 = k\text{-}N\text{+}1$ is the first stage inside estimation, and j is the moving counter inside the estimation window. In general, the determination of system noise aims to guarantee the accuracy of the filtering process. To overcome estimation error due to external disturbances (turbulence), a moving time window (N) for robust and adaptive estimation of air data that is insensitive to variation in the monitoring is process used. Note that the proposed method requires tuning a $\mathbf{Q}$ matrix whose noise statistics are unknown. From the proposed system knowledge, it is clear that there are possibilities for unexpected external disturbances to the system, such as atmospheric turbulence. Therefore, a moving window with defined length N is considered. If $k > N$, the newest information will be weighted to locate the significance of newly received data. Furthermore, the weight value will be attenuated exponentially. Hence, the improved version of the $\hat{\mathbf{C}}_{ek}$ is written as,

$$\hat{\mathrm{C}}_{ek} = \lambda \hat{\mathrm{C}}_{ek-1} + \frac{1-\lambda}{1-\lambda^N}\left(e_k e_k^T - \lambda^N e_{k-N} e_{k-N}^T\right) \tag{28}$$

where λ is the attenuation factor. The improved $\hat{\mathbf{C}}_{ek}$ will be placed into the Kalman gain matrix to strengthen the robustness of the EW-AEKF because of the filter gain tuned to the noise fluctuations. Hence, the adaptive estimate of the process noise covariance matrix is given by

$$\hat{\mathrm{Q}}_k = \mathrm{K}_k \mathrm{C}_{ek} \mathrm{K}_k^T \tag{29}$$

Based on the adaptive $\mathbf{Q}$ matrix estimation, the filter gain ($\mathbf{K}_k$) was improved to strengthen the robustness of the filtering algorithm. Note that the proposed method considers tuning of the $\mathbf{Q}$ matrix only. Tuning of the $\mathbf{R}$ matrix is not required for the proposed algorithm as the measurement sensor's noise covariance is known, reliable, and less affected by external disturbances. Furthermore, avoiding the $\mathbf{R}$ matrix tuning excludes the additional computations.

4.0 PADS-FDD algorithm

In this section, a simple fault detection (FDD) logic is presented to detect any type of fault on the primary air data sensors (PADS) considered for the proposed work. The FDD scheme is shown in Fig. 2.

In general, residual-based FDD carries the fault information irrespective of fault types. In this study, the residuals for the FDD scheme are calculated offline to simulate various types of fault scenarios by injecting faults into the fault-free flight data measurements. In order to detect a fault, the residuals are used as a fault detector or vector. The residuals calculated for the proposed PADS-FDD algorithm were

https://doi.org/10.1017/aer.2023.32 Published online by Cambridge University Press

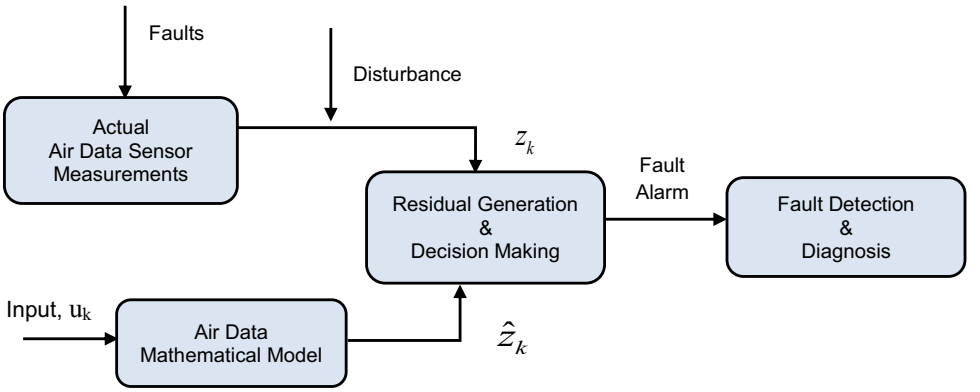

Figure 2. *PADS-FDD scheme.*

calculated using the actual or redundant physical sensor measurements and the estimated data, i.e. the analytically redundant measurements. For better FDD performance, a fault model is framed, which is a formal representation of the knowledge of possible faults and how they influence the process. As far as air data sensor fault detection is concerned, the fault types will vary depending on the various flight conditions and sensor positioning on the aircraft. For example, Pitot tube ports are usually blocked by foreign objects such as the entry of insects when aircraft are on the ground, icing at high altitudes, volcanic ashes, rainwater entry, etc. Note that in all these cases, the Pitot tubes will be blocked, which may cause frozen output or a stuck fault to occur. A fault model (f_k) includes each sensor's data for fault types such as stuck, bias, drift and increased noise faults under abnormal conditions, including adverse weather conditions and atmospheric turbulence. The faulty sensor output can be presented as

$$Z_k = z_k + f_k \tag{30}$$

where Z_k is the faulty sensor data, with an added fault model at time t being the fault-free sensor data (z_k). It is assumed that the estimated air data is free of faults throughout the FDD process. A residual is a computed quantity that is used to alarm if a fault is present in the supervised air data sensors (PADS) or not. The residuals (e_k) of each sensor category of the air data system are calculated using the more general form of the residual equation as follows:

$$|e_k| = \left|Z_k - \hat{z}_k\right| \tag{31}$$

where$|e_k|$ is the absolute value of the residual signal, which can be explored using Equation (2) to differentiate each category of faulty sensors in the air data system. It can be presented as,

$$\begin{cases} \left|e_{U_t}\right| = \left|(U_t + f_i) - \hat{U}_t\right| \\ |e_\alpha| = \left|(\alpha + f_i) - \hat{\alpha}\right| \\ \left|e_\beta\right| = \left|(\beta + f_i) - \hat{\beta}\right| \end{cases} \tag{32}$$

where U_t,α, and β are the physical air data sensor measurements such as airspeed, AOA and AOSS, respectively, and f_i represents the fault added to the i^{th} physical sensor measurements at time t. In order to detect a fault, a predetermined threshold (J_T) is assigned to each sensor. The objective of the proposed method is to minimise the number of false alarms and avoid false detections in fault-free conditions. When setting a fault detection threshold, it is crucial to keep the false alarm rate (FAR) and the missed detection rate (MDR) under control. For example, a too-low threshold value will lead to an increased false alarm rate, and a too-high threshold will lead to more missed detections [28]. Note that increased false alarms indicate a poorly designed mathematical model, which may enable unwanted control actions that could adversely affect the system's performance. The rationale behind this philosophy is that we

https://doi.org/10.1017/aer.2023.32 Published online by Cambridge University Press

Figure 3. *X-Plane flight simulator setup.*

only focus on detecting faults that may help to design a reliable FDD for the application of aircraft control systems related to the air data system. An alarm signal (F_A) is used to indicate faulty situations using binary decision logic (0 and 1). When a fault occurs, the F_A will set logic 1. When there are no faults, the F_A will be set to logic 0. If any of the air data sensor residual values exceed the J_T, F_A will be set to 1, and a fault is detected. It can be represented as

$$\begin{aligned} \left|e_k^i\right| &< J_T, \text{ Fault alarm, } F_A \text{ set to } 0 \\ \left|e_k^i\right| &> J_T, \text{ Fault alarm, } F_A \text{ set to } 1 \end{aligned} \tag{33}$$

where $\left|e_k^i\right|$ is the absolute (modulus) of the residuals of i^{th} sensor of the air data cluster (U_t, α, β) considered to be a non-negative quantity without regard to its sign. In Section 5, we will present the various fault scenarios of the sensors to simulate the proposed PADS-FDD algorithm.

5.0 Experimental setup and simulation results

In this study, we used the X-Plane 10 flight simulator to carry out an experimental flight and generate flight sensor data for the proposed PADS-FDD. The simulation setup consists of the X-Plane version 10.32 simulator software, a Logitech Extreme Pro Joystick, a Mobile Workstation Laptop with a Core i7-6820HQ CPU, and an Nvidia Quadro graphics card used as shown in Fig. 3. X-Plane is a comprehensive and powerful flight simulator that can simulate the flying characteristics of aircraft accurately. In addition to being used for certified flight simulations in accordance with FAA regulations, X-Plane has been the subject of numerous studies [29–32]. The turbulence generated by the X-Plane simulator is based on overlaid sinusoidal waves with various frequencies. The aircraft models provided in the X-Plane simulator are based on the blade element theory (the airplane is divided into many small elements, and the forces acting on each element are calculated with a frequency of several hertz). It includes the effects of atmospheric disturbances such as turbulence, wind shear, wind gust, etc. For different layers of the atmosphere, we can set the wind speed, its direction and the turbulence level. X-Plane can transmit and receive flight data using the User Datagram Protocol (UDP). The data I/O window of the X-Plane is employed to choose the parameters that will be communicated to Simulink in the form of data packets. UDP is used for data transmission between Simulink and X-Plane. We ran the simulator via UDP communication incorporated in Matlab/Simulink and recorded flight data under various turbulence conditions. To obtain flight data, a software-in-the-loop (SITL) simulation was performed with a Boeing B737-800 aircraft that is readily available in the X-Plane's aircraft folder. The B737-800 aircraft is a large fixed-wing commercial transport aircraft with twin jet engines. To complete the autopilot's fundamental operational loops, including pitch control loop (PCL), roll control loop (RCL), altitude hold

https://doi.org/10.1017/aer.2023.32 Published online by Cambridge University Press

Table 1. *Comparison of filter estimation performance*

Parameter	Unit of Measurement	RMSE	
		EKF	EW-AEKF
True airspeed (U_t)	m/s	2.328340	0.092810
Angle-of-attack (α)	rad	0.007377	0.000019
Angle-of-sideslip (β)	rad	0.007697	0.000020

(AH) and heading hold (HH), the controller receives feedback from the X-Plane flight data. The PID controller was used to implement each of these loops. UDP send and receive blocks were accessed with two independent unidirectional transmissions and an Internet Protocol (IP) address. For the UDP connection between Matlab/Simulink and X-Plane, the IP address used was 127.0.0.1 with the output ports 49,000 and 49,004. The frame rate was set to 50 packets per second (pps) during flight simulation.

The flight data was collected with the required variables. Data outputs are recorded by using the data output option in X-Plane with a text (.txt) file. The flight simulation was carried out with take-off, climb and cruise phases under atmospheric turbulence. The atmospheric turbulence magnitude was set to 2 using the weather setting under the environment tab, as shown in Fig. 4. Before implementing the proposed approach, the accuracy and stability of the filtering mechanisms were studied to verify the air data estimation algorithms using traditional EKF and the proposed EW-AEKF.

5.1 Filter estimation performance results

In this subsection, we present the simulation test results of conventional EKF and adaptive EKF (EW-AEKF) to compare and verify the estimation performance. For the estimation of air data, the filtering performance of a so-called non-linear filter (EKF) and EW-AEKF was tested under abrupt environmental variations such as atmospheric turbulence. The EKF performance was found to be insufficient due to convergence errors. Therefore, an adaptive version of EKF (EW-AEKF) is preferred to estimate air data and detect sensor faults. Figures 5 and 6 show the estimation plots of air data (true airspeed, angle-of-attack, and angle-of-sideslip) under fault-free conditions. To test the filters, the simulated flight data was logged with moderate atmospheric turbulence (turbulence magnitude of 2) at an altitude of 5,000m.

As can be seen, the estimation performance of EW-AEKF is better than the estimation using EKF in terms of filter convergence error. Note that the filter estimation error is crucial for model-based FDD methods to ensure reliable estimates of the aircraft parameters. The estimation performance was compared with the root mean square error (RMSE) of the filters and is presented in Table 1.

5.1.1 Robustness analysis using Monte Carlo simulations

In this section, experiment results using Monte Carlo Simulations (MCS) are presented for the performance evaluation of the developed FDD scheme with respect to the uncertainty acting on the system. The analysis using MCS represents a further method for estimating the reliability and robustness of the FDD scheme [33]. The simulation of different fault-free and faulty data sequences was carried out with various turbulence conditions. The MCS was performed by varying the parameters of the kinematic model developed for the proposed algorithm by exploiting the MATLAB platform. Table 2 summarises the results obtained by considering the EW-AEKF estimation for the air data sensor FDD. As shown in Fig. 7, the mean and standard deviations of estimation error are within the acceptable level. The performance of the FDD method was evaluated on a number of Monte Carlo runs equal to 2,000. Based on the outcome of MCS, performance metrics such as false-alarm rate (FAR) and missed detections are analysed for the fault-free and each fault case. With the proper design of the fault detection filter and

https://doi.org/10.1017/aer.2023.32 Published online by Cambridge University Press

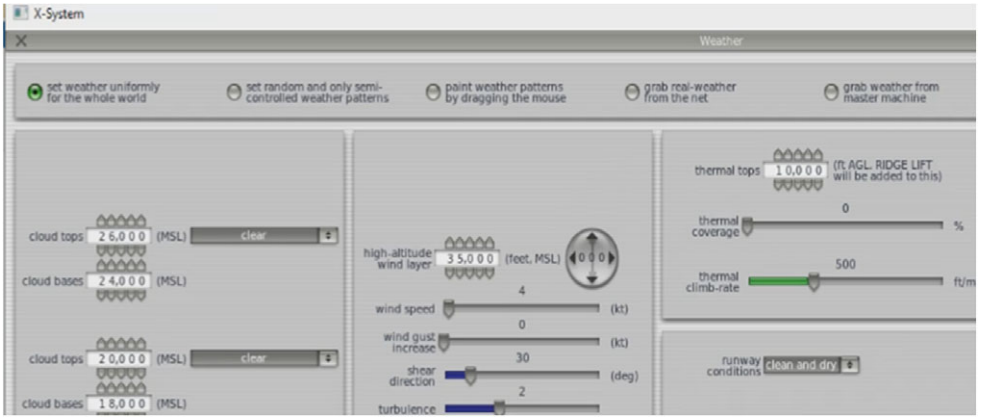

Figure 4. *Environmental setup using X-Plane simulator.*

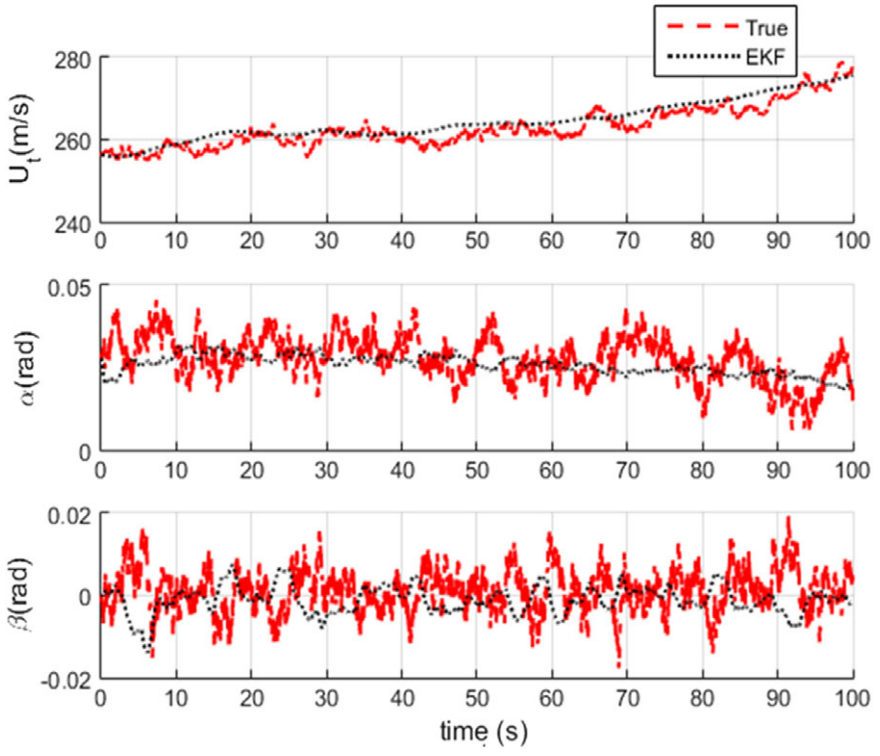

Figure 5. *Air data estimation using EKF.*

choice of the FDD thresholds, we achieved FDD with better detectability and a FAR of 0.8% for airspeed, 0.5% for AOA, and 1.75% for AOSS. The results demonstrate that the robustness of the proposed FDD method can be effectively analysed using Monte Carlo simulations.

https://doi.org/10.1017/aer.2023.32 Published online by Cambridge University Press

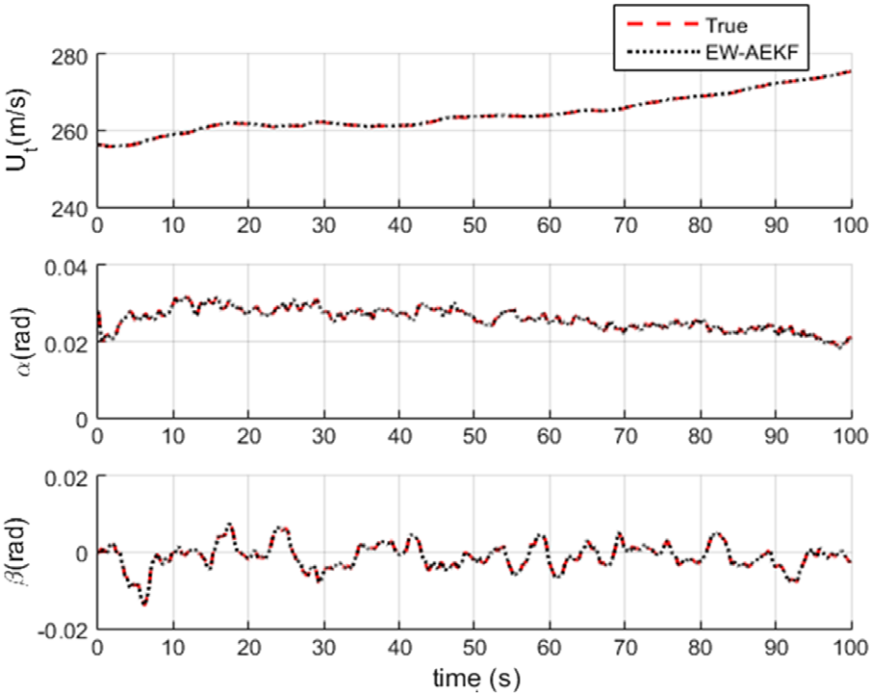

Figure 6. *Air data estimation using EW-AEKF.*

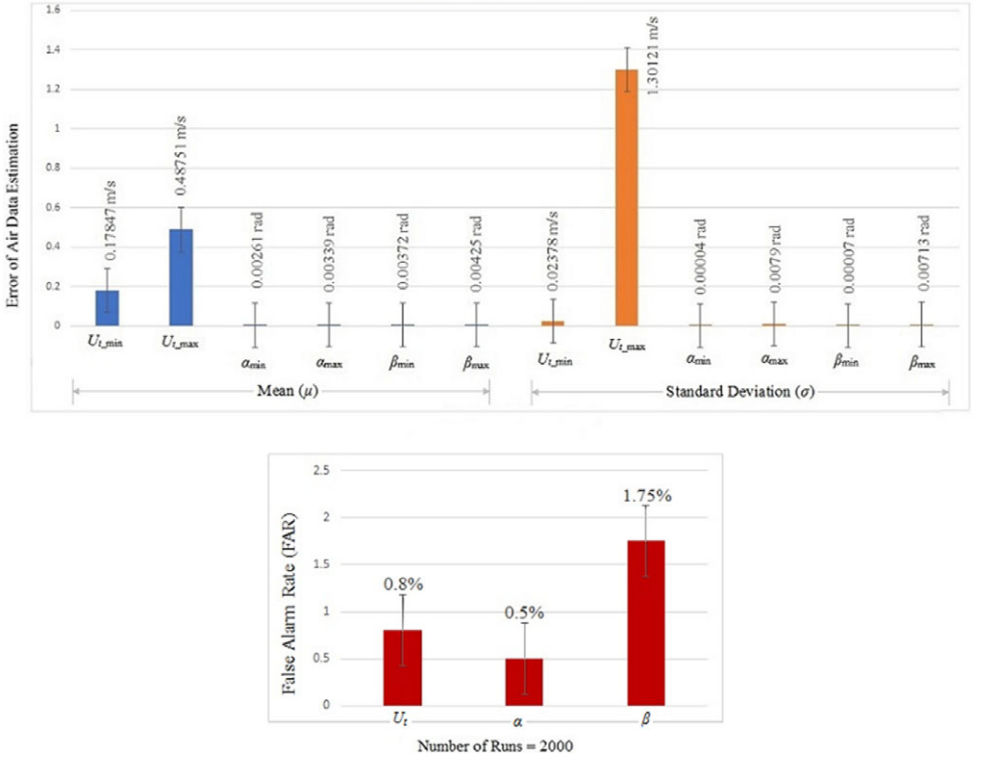

Figure 7. *MCS results of estimation error and FAR.*

https://doi.org/10.1017/aer.2023.32 Published online by Cambridge University Press

Table 2. *Monte-Carlo outcome of air data estimation and FDD performance*

Variable	Mean of Error (μ)		Standard Deviation of Error (σ)		FAR
	Min.	Max.	Min.	Max.	(%)
Airspeed (U_t)	0.17847m/s	0.48751m/s	0.02378m/s	1.30121m/s	0.8
AOA (α)	0.00261rad	0.00339 rad	0.00004rad	0.00790rad	0.5
AOSS (β)	0.00372rad	0.00425rad	0.00007rad	0.00713rad	1.75

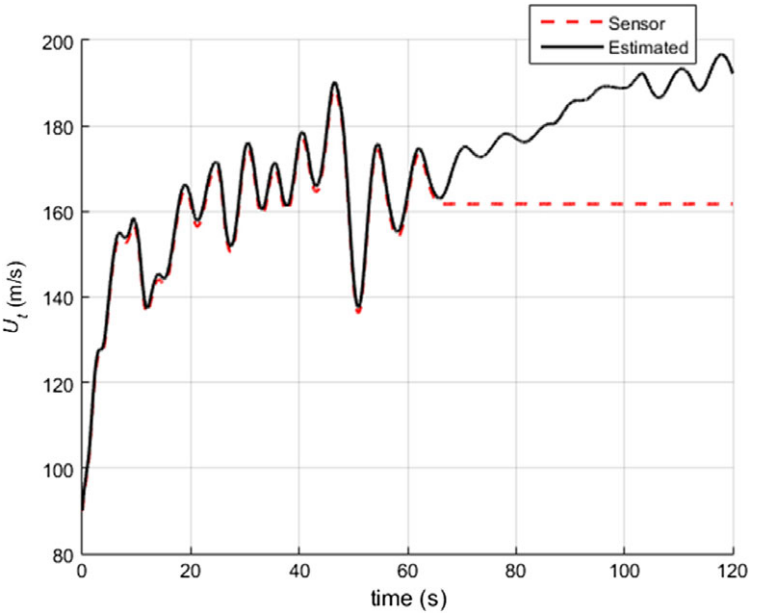

Figure 8. *Airspeed sensor stuck fault at $t = 66$sec.*

5.2 PADS-FDD results using simulated flight sensor data

In this subsection, we presented the results of the PADS-FDD algorithm using simulated flight sensor data of a B737-800 aircraft with a turbulence magnitude of 2 at an altitude of 10,668m. To validate the algorithm using captured flight data, the EW-AEKF estimated air data, and the physical sensor data of the aircraft used. Note that the actual air data sensor measurements are not used in the filtering procedure and are used only as a comparison reference with the estimated air data to detect and diagnose faults. The PADS-FDD results for the various fault scenarios under atmospheric turbulence were considered. The most common fault that occurs on Pitot tubes is the blockage fault, which leads to a stuck or frozen output on the airspeed indications. Figures 8 and 9 show the Pitot tube blockage (stuck) fault in the flight sensor data at time $t = 66$sec.

As can be noticed, the absolute value of the residual signal (e_{U_t}) exceeds the predetermined threshold of 2m/s at time $t = 66$sec, and it jumps beyond 30m/s. Hence, the fault is detected. During the sensor fault, the RMSE of the filter (EW-AEKF) is 15.7612m/s. Note that the fixed threshold value is related to the permissible error limit of an airspeed indicating system as mentioned in the EASA specifications. Figures 10 and 11 show the simulation results of the drift fault and residuals of the airspeed sensor.

In Fig. 10, the drift fault of the airspeed sensor is presented by injecting the fault in the physical airspeed sensor measurements at time $t = 70$sec.

Drift fault is a condition where the measurement error rises over time, which originates from the loss of the sensor's sensitivity. In Fig. 11, the residual (e_{U_t}) exceeds the 2m/s threshold and reaches

https://doi.org/10.1017/aer.2023.32 Published online by Cambridge University Press

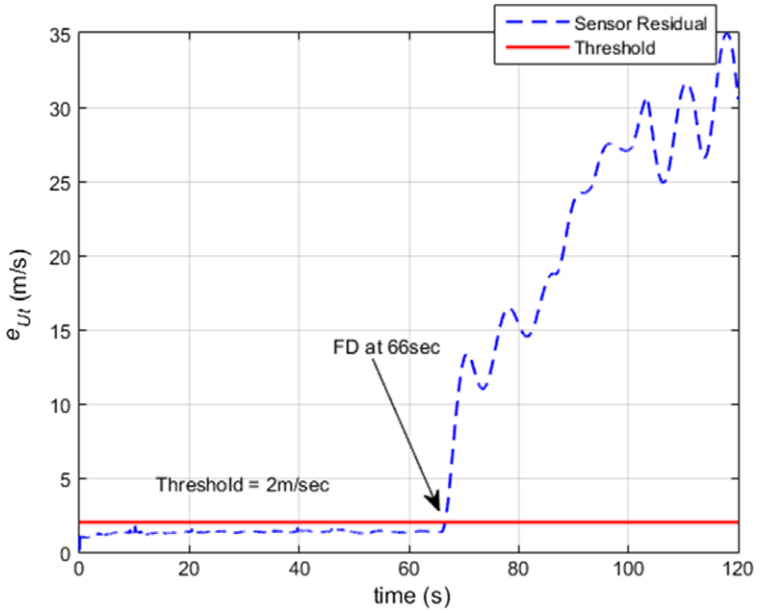

Figure 9. *Airspeed sensor residual during stuck fault.*

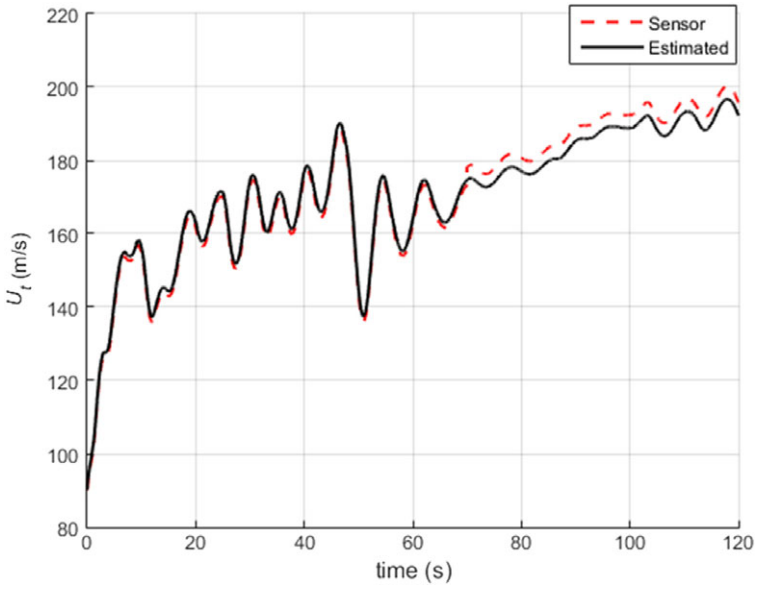

Figure 10. *Airspeed sensor drift fault at $t = 70$sec.*

beyond 3.5 m/s, which is not acceptable. The RMSE of the filter during the airspeed sensor drift fault is 2.5129m/s. In Figs 12, 13, 14, and 15, the airflow angles (α and β) fault detection is presented as a bias fault, which is the most common fault experienced by the commercial aircraft vane type α and β sensors. A bias fault is the steady offset error between the actual and measured values. The results are shown below.

In Fig. 12, the bias fault is introduced to the physical angle-of-attack sensor measurements at time $t = 65$sec. The absolute value of the residual signal exceeds the predetermined threshold of 0.008rad. As a result, the fault is detected at $t = 65$sec. Figure 13 shows the residual variations during bias fault

https://doi.org/10.1017/aer.2023.32 Published online by Cambridge University Press

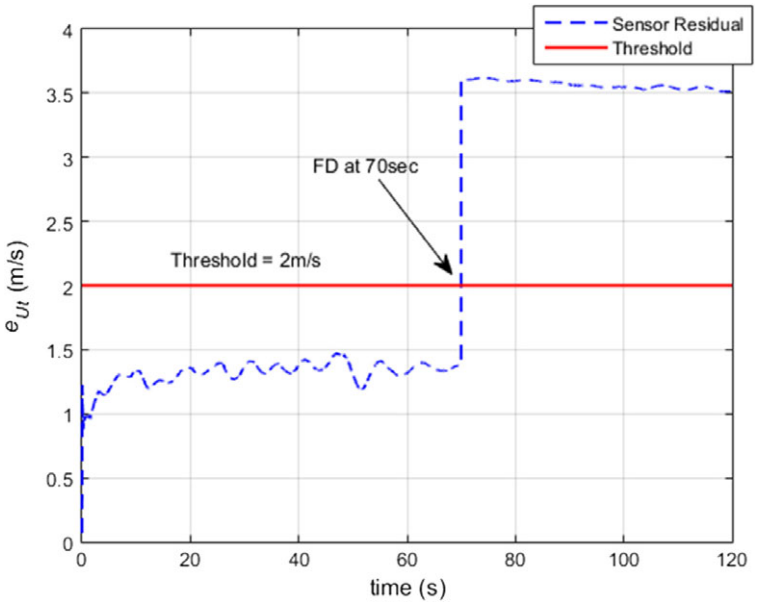

Figure 11. *Airspeed sensor residual during drift fault.*

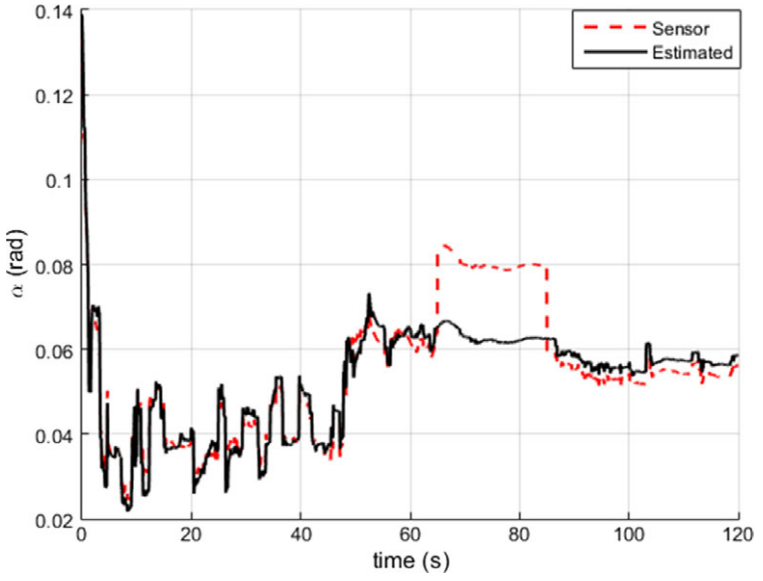

Figure 12. *Angle-of-attack (α) sensor bias fault at $t = 65$sec.*

on the angle-of-attack (α) sensor. Figure 14 shows the bias fault on the angle-of-sideslip (β) sensor at time $t = 60$sec.

In Fig. 15, the residuals after the bias fault on the β sensor, which exceed the threshold value of 0.0025rad, is presented. The RMSE of the filter during α and β sensors bias faults is 0.0074rad and 0.0012rad, respectively.

In Figs 16, 17, 18, 19, 20, and 21, an increased noise fault on the air data sensors is introduced under the atmospheric turbulence. During turbulence, the air data sensors' noise increases significantly because of the heavy airflow distortion. The turbulence magnitude of 3 was set in the flight simulator weather setup window. The results are shown below:

https://doi.org/10.1017/aer.2023.32 Published online by Cambridge University Press

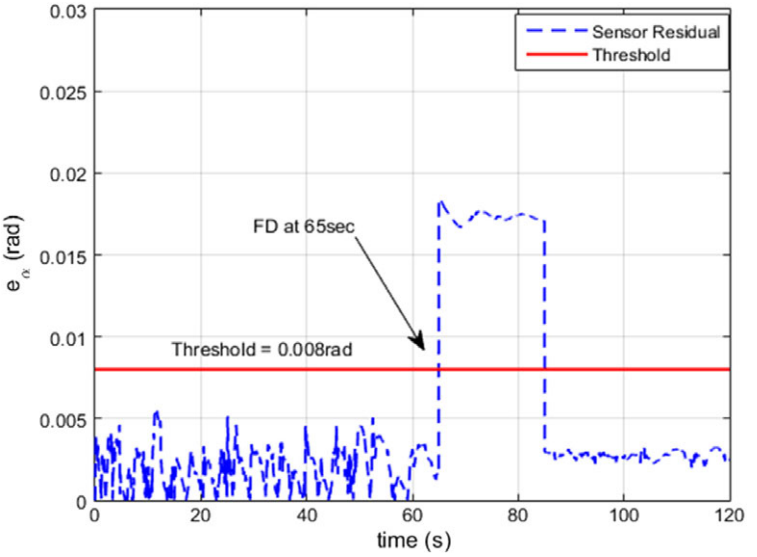

Figure 13. *α sensor residual during bias fault.*

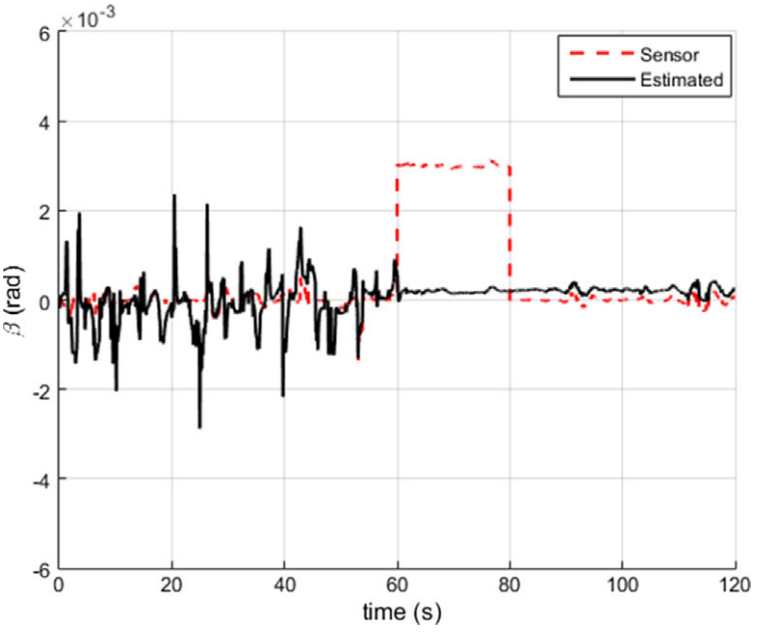

Figure 14. *β sensor bias fault at t = 60sec.*

Figure 16 shows the increased noise fault on the airspeed sensor under external disturbance (turbulence). The residual variations found in Fig. 17 show that the fault detected at time $t = 141.9$sec, and the residuals surpass the fixed threshold value of 2m/s. As can be noticed, the airspeed sensor residual jumps beyond 16m/s after the occurrence of the fault. The RMSE of the filter during the fault is 3.5572m/s.

As seen in Figs 18 and 20, increased noise faults occurred on α and β sensor measurements at time $t = 141.95$ and $t = 141.9$sec, respectively. As can be noticed, heavy airflow distortions caused by the increased turbulence magnitude on the rotating vane type α and β sensors cause an increased noise fault. In Figs 19 and 21, the AOA (α) and AOSS (β) sensor residuals indicate the occurrence of increased noise

https://doi.org/10.1017/aer.2023.32 Published online by Cambridge University Press

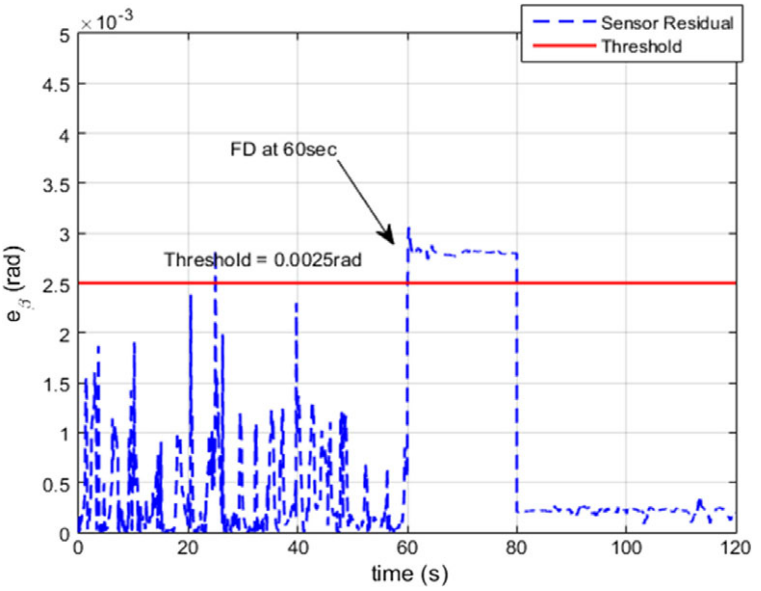

Figure 15. *Angle-of-sideslip (β) sensor residual at $t = 60$sec.*

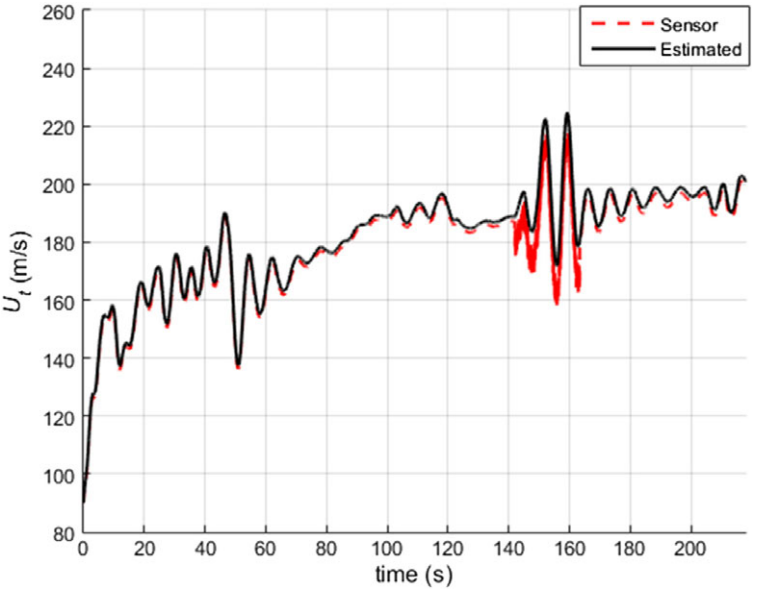

Figure 16. *Airspeed sensor increased noise fault at $t = 141.9$sec.*

faults when they exceed the fixed thresholds of 0.01 and 0.005rad, respectively. The RMSEs of the filter during α and β sensor noise faults are 0.0039 and 0.0021rad, respectively.

6.0 Conclusions

In this paper, fault detection and diagnosis of air data sensors are presented using estimated air data in the presence of moderate atmospheric turbulence. The mathematical model was developed using aircraft kinematics, which excludes the forces and moments of the aircraft. The proposed PADS-FDD algorithm

https://doi.org/10.1017/aer.2023.32 Published online by Cambridge University Press

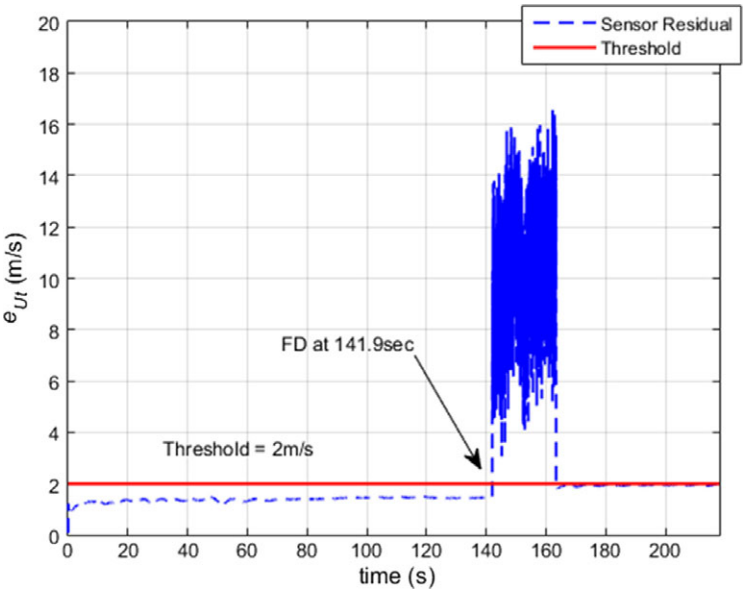

Figure 17. *Airspeed sensor residuals after noise fault.*

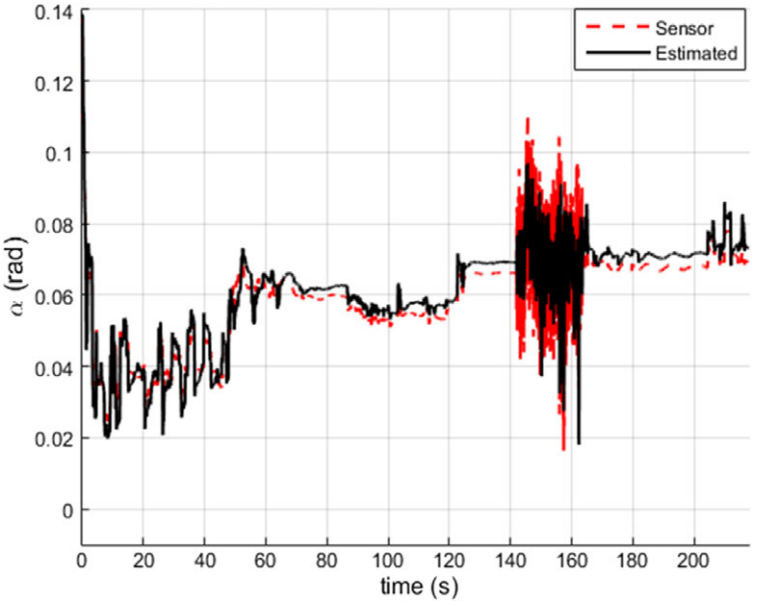

Figure 18. *α sensor increased noise fault at t = 141.95sec.*

simulated various fault scenarios using the MATLAB platform. In order to estimate reliable air data, the exponentially weighted adaptive Kalman filter (EW-AEKF) was designed and implemented with a lower computational load. The estimation performance of the EW-AEKF was found to be consistent even in a turbulent environment. The estimated data is used to generate residual signals and detect the actual air data sensor faults using a simple residual equation. Before validating the FDD algorithm, a general extended Kalman filter (EKF) and an adaptive version of the EKF (EW-AEKF) were designed to verify the filter consistency checks. On comparison with the general EKF, the EW-AEKF has better estimation performance in terms of less estimation error achieved for the true airspeed, AOA and AOSS, which are

https://doi.org/10.1017/aer.2023.32 Published online by Cambridge University Press

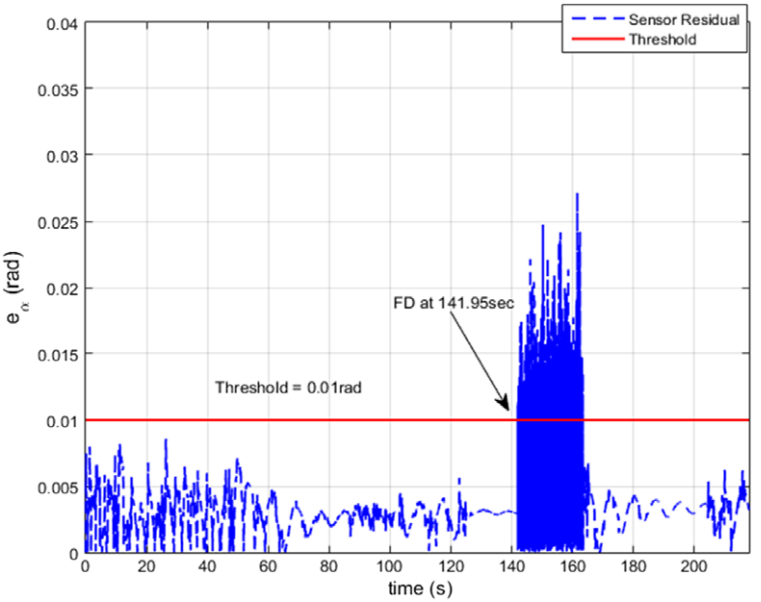

Figure 19. *α sensor residuals after noise fault.*

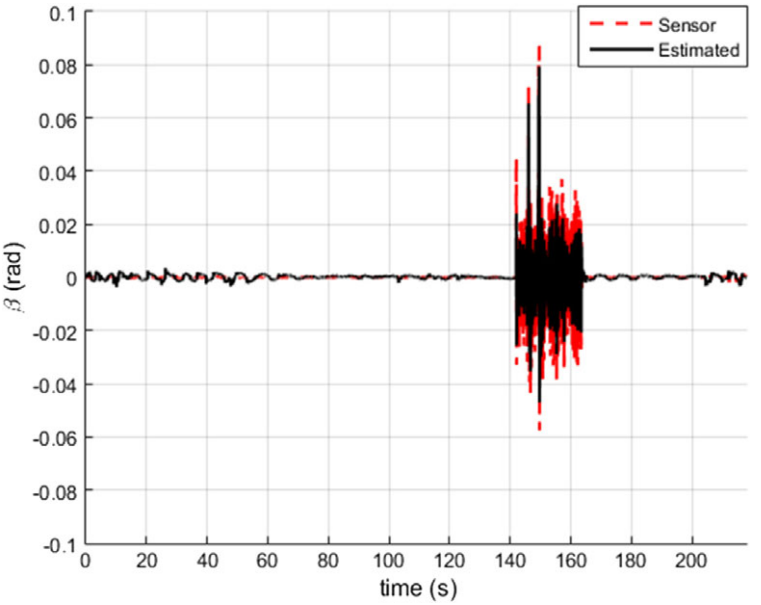

Figure 20. *β sensor increased noise fault at t = 141.9sec.*

0.092810m/s, 0.000019rad and 0.000020rad, respectively. An extensive experiment was carried out by exploiting Monte Carlo simulations for assessing the overall capabilities of the developed EW-AEKF-based PADS-FDD method in the presence of atmospheric turbulence and uncertainties. The outcome of the Monte Carlo simulation shows that the reliability and robustness properties of the system were achieved with lower false alarm probabilities. The PADS-FDD algorithm was validated with simulated flight data under moderate atmospheric turbulence. The results show that the proposed algorithm can provide a reliable FDD for air data sensor fault-tolerant control systems with less error and computational complexity.

https://doi.org/10.1017/aer.2023.32 Published online by Cambridge University Press

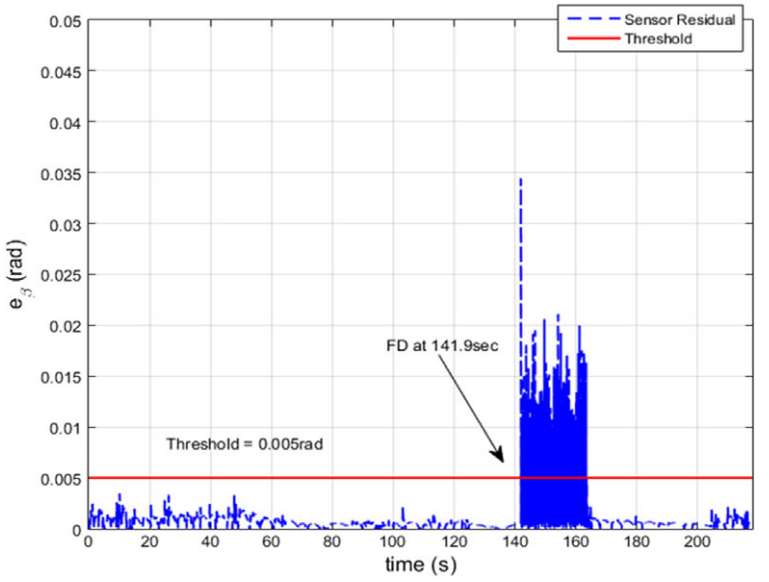

Figure 21. *β sensor residuals after noise fault.*

The future work intends to carry out a real-time flight test with an air data sensor FDD while an aircraft is flying under different atmospheric turbulence intensities to show the effectiveness of the proposed algorithm. However, due to safety concerns, verification of the algorithm on a manned aircraft is not recommended. Hence, it is recommended to verify the same on unmanned platforms such as fixed-wing drones.

References

[1] Final report on the accident on 1 June 2009 to the Airbus A330-203, 2012, https://www.bea.aero/docspa/2009/f-cp090601.en/pdf/f-cp090601.en.pdf

[2] Palmer, C. The Boeing 737 Max Saga: automating failure, *J. Eng.*, 2020, **6**, (1), pp 2–3, doi: 10.1016/j.eng.2019.11.002

[3] Aircraft accident investigation report of the crash on 29 October 2018 to the B737 Max 2019, http://knkt.dephub.go.id/knkt/ntsc_aviation/baru/2018/PKLQP%20Final%20Report.pdf.

[4] Sobhani-tehrani, E. and Khorasani, K. *Fault Diagnosis of Nonlinear Systems Using a Hybrid Approach*, Springer, 2009, New York, US.

[5] Lu, P., Van Kampen, E.J., De Visser, C.C. and Chu, Q.P. Nonlinear aircraft sensor fault reconstruction in the presence of disturbances validated by real flight data, *Cont. Eng. Pract.*, 2016, **49**, pp 112–128, doi: 10.1016/j.conengprac.2016.01.012

[6] Berdjag, D., Zolghadri, A. and Cieslak, J. Fault detection and isolation of aircraft air data/inertial system, Proceedings of the European Conference for Aerospace Sciences, 2013, pp 317–332, doi: 10.1051/eucass/201306317

[7] Gururajan, S., Fravolini, M., Rhudy, M. and Moschitta, A. Evaluation of Sensor Failure Detection, Identification and Accommodation (SFDIA) Performance Following Common-Mode Failures of Pitot Tubes, September 2014, SAE Technical Paper, doi: 10.4271/2014-01-2164

[8] Swischuk, R. and Allaire, D. A machine learning approach to aircraft sensor error detection and correction, *ASME J. Comp. Inf. Sci. Eng.*, 2019, **19**, (4), 041009, doi: 10.1115/1.4043567

[9] Ossmann, D. and Joos, H.D. Enhanced detection and isolation of angle of attack sensor faults, Proceedings of the AIAA GNC Conference, 2016, pp 1–16, doi: 10.2514/6.2016-1135

[10] Marco, A., Massimiliano, M., Immacolata, N., Federico, C. and Adolfo, S. An SFDI observer–based scheme for a general aviation aircraft, *Int. J. App. Math. Comp. Sci.*, 2015, **25,** (1), pp 149–158, doi: 10.1515/amcs-2015-0011

[11] Antonio, V., Federico, C., Nicola, G., Luca, G. and Leopoldo, V. An innovative angle of attack virtual sensor for physical-analytical redundant measurement system applicable to commercial aircraft, *Adv. Sci. Tech. Eng. Syst. J*, 2021, **6**, (1), pp 698–709, doi: 10.25046/aj060176

[12] Varga, A., Ossmann, D. and Joos, H.D. A fault diagnosis based reconfigurable longitudinal control system for managing loss of air data sensors for a civil aircraft, *IFAC Proc.*, 2014, **47,** (3), pp 3489–3496, doi: 10.3182/20140824-6-ZA-1003.00672

[13] Alcalay, G., Seren, C., Hardier, G., Delporte, M. and Goupil, P. An adaptive extended Kalman filter for monitoring and estimating key aircraft flight parameters, *IFAC*, 2018, **51**, (24), pp 620–627, doi: 10.1016/j.ifacol.2018.09.640

https://doi.org/10.1017/aer.2023.32 Published online by Cambridge University Press

[14] Zahed, M.J.H, Alabsi, M.I., Fields, T. and Hetrick, D. Virtual sensor development for actual sensor fault detection and flight parameter estimation in real time, Conf. Proceedings of the AIAA Scitech Forum, 2020, doi: 10.2514/6.2020-0510
[15] Kilic, U. and Unal, G. Sensor fault detection and reconstruction system for commercial aircrafts, Aeronaut. J., 2022, 126, (1299), pp 889–905.
[16] Hazbon, O., Gutierrez, L., Bil, C., Napolitano, M. and Fravolini, M. Digital twin concept for aircraft system failure detection and correction, Proceeding of the AIAA Conference, 2019, doi: 10.2514/6.2019-2887
[17] Lu, C., Li, R.B., Liu, J.Y. and Lei, T.W. Air data estimation by fusing navigation system and flight control system, J. Navig., 2018, 71, (5), pp 1231–1246, doi: 10.1017/S037346331800022X
[18] Mohamed, M. and Joy, N. Online estimation of aircraft flow angles in turbulent atmosphere, IFAC Conf., 2020, 53, (1), pp 597–601, doi: 10.1016/j.ifacol.2020.06.100
[19] Lu, P., Van Kampen, E.J., De visser, C. and Chu, Q.P. Air data sensor fault detection and diagnosis in the presence of atmospheric turbulence: theory and experimental validation with real flight data, *IEEE Trans. Cont. Sys. Tech.*, 2021, **29,** (5), pp. 2255–2263, 10.1109/TCST.2020.3025725.
[20] Julier, S.J. and Uhlmann, J.K. A new extension of the Kalman filter to nonlinear systems, Proceedings of the SPIE Signal Proc., Sensor Fusion, and Target Recognition, vol. 3068, 1997, doi: 10.1117/12.280797
[21] Guo, D., Zhong, M. and Zhou, D. Multi-sensor data-fusion-based approach to airspeed measurement fault detection for unmanned aerial vehicles, *IEEE Trans. Inst. Meas.*, 2018, **67**, (2), pp 317–327, doi: 10.1109/TIM.2017.2735663
[22] https://www.easa.europa.eu/sites/default/files/dfu/cs-25_amendment_27.pdf
[23] https://www.caa.co.uk/media/vkdl44xb/caa-cs-25-amendment-26-initial-airworthiness.pdf
[24] Stevens, B.L. Lewis, F.L. and Johnson, E.N. *Aircraft Control and Simulation: Dynamics, Controls Design, and Autonomous Systems*, Wiley, 2015, US.
[25] Mulder, J.A., Chu, Q.P., Sridhar, J.K., Breeman, J.H. and Labanm, M. Non-linear aircraft flight path reconstruction review and new advances, Elsevier Prog. Aero. Sci., 1999, 35, pp 673–726, doi: 10.1016/S0376-0421(99)00005-6
[26] Prabhu, S. and Anitha, G. An innovative analytic redundancy approach to air data sensor fault detection, *Aeronaut. J.*, 2020, **124,** (1273), pp 346–367, doi: 10.1017/aer.2019.143
[27] Mukherjee, M., Das, M. and Sadhu, S. Q-adaptive extended Kalman filter for nonlinear systems with unknown noise statistics, 15th IEEE India Council International Conference, 2018, pp 1–6, doi: 10.1109/INDICON45594.2018.8987109
[28] Chen, J. and Patton, R.J. *Robust Model-Based Fault Diagnosis for Dynamic Systems*, Kluwer Academic Publishers, 1999, Boston, USA.
[29] Bittar, A., Figuereido, H.V., Guimaraes, P.A. and Mendes, A.C. Guidance software-in-the-loop simulation using X-plane and Simulink for UAVs, International Conference on Unmanned Aircraft Systems (ICUAS), 2014, pp 993–1002, doi: 10.1109/ICUAS.2014.6842350
[30] Horri, N. and Pietraszko, M.A. Tutorial and review on flight control co-simulation using Matlab/Simulink and flight simulators, *MDPI Autom. J.*, 2022, **3**, (3), pp 486–510. Survey Review, doi: 10.3390/automation3030025
[31] Jamadagni, C.S., Chethan, C.U., Jeppu, Y., Kamble, S.B. and Desai, V.H. System simulation approach for helicopter autopilot, International Conference on Contemporary Computing and Informatics (IC3I), 2014, pp 404–408, doi: 10.1109/IC3I.2014.7019616
[32] Silva, W.R., Da Silva, A.L. and Grundling, H. Modelling, simulation and control of a fixed-wing Unmanned Aerial Vehicle (UAV), Proceedings of the 24th ABCM International Congress of Mechanical Engineering, 2017, pp 3–8, doi: 10.26678/ABCM.COBEM2017.COB17-2703
[33] Benini, M., Bonfù, M., Castaldi, P., Geri, W. and Simani, S. Design and analysis of robust fault diagnosis schemes for a simulated aircraft model, *J. Control Sci. Eng.*, 2008, doi: 10.1155/2008/274313

Appendix

https://doi.org/10.1017/aer.2023.32 Published online by Cambridge University Press

Cite this article: Prabhu S. and Anitha G. (2023). Robust fault detection and diagnosis of primary air data sensors in the presence of atmospheric turbulence. *The Aeronautical Journal*, **127**, 2023–2046. https://doi.org/10.1017/aer.2023.32